A Charged Active Contour based on Electrostatics

Ronghua Yang, Majid Mirmehdi, Xianghua Xie

Department of Computer Science, University of Bristol, Bristol, BS8 1UB, UK
`{ronghua,majid,xie}@cs.bris.ac.uk`

Abstract. We propose a novel active contour model by incorporating particle based electrostatic interactions into the geometric active contour framework. The proposed active contour, embedded in level sets, propagates under the joint influence of a boundary attraction force and a boundary competition force. Unlike other contour models, the proposed vector field dynamically adapts by updating itself when a contour reaches a boundary. The model is then more invariant to initialisation and possesses better convergence abilities. Analytical and comparative results are presented on synthetic and real images.

1 Introduction

Ever since the introduction of the parametric snake [1], deformable models have received much attention for region segmentation and object detection. The geodesic active contour [2] is a significant improvement over the parametric snake in that it can naturally handle topological changes. However, it still suffers from drawbacks such as edge leakage and sensitivity to initialisation. There have been many efforts in improving both parametric and geometric snakes, for example by introducing region-based features to make the model more robust to initial conditions [3–5]. One significantly improved parametric model is the Gradient Vector Flow (GVF) snake [6] which uses a bi-directional external force field that provides long-range capture of object boundaries from either side. One of its main drawbacks however is that the contour does not propagate where the vector flows are tangent to the contour or diverge within a neighbourhood. One improvement of the geometric snake model is the GVF geodesic snake [7] which integrates the GVF with a geometric contour formulation and introduces an adaptive balloon force to help propagate the contour when the vector flows are tangent to the contour. This allows it to outperform the GVF snake while also benefitting from topological freedom. However, it is still unable to propagate through the points where the GVF field has large divergence which form in homogeneous areas depending on object topology. Therefore, the contours must be initialised with great care in order to avoid getting trapped at these points.

Recently, a new formulation for a "deformable model" based on charged particle dynamics, founded on electrostatics and particle movements, and called the Charged Particle Model (CPM), was introduced by Jalba et al. [8]. CPM

can capture object boundaries over the entire image with a set of free charged particles. These are attracted by object boundaries via an image-based force field, while at the same time being repelled from one another by a charged particle-based force which constantly imposes on the particles to advance them along object boundaries. While an initialization step is still required, it is certainly less pivotal than in the contour model. However, this particle model a) can not guarantee continuous and closed final contours, b) does not stabilise as there is no effective stopping term, and c) is computationally intensive.

In order to overcome the common drawbacks in the traditional deformable contour model and the deformable particle model, we propose a new framework by introducing particle based electrostatics into active contour propagation that incorporates the advantages of both contour and particle based models. We refer to this as CACE, a *C*harged *A*ctive *C*ontour based on *E*lectrostatics. CACE can detect object boundaries via contour propagation under the influence of a bi-directional force field that simulates the electrostatic interaction between an image-derived point charge field and a charged contour. In other words, the force consists of boundary attraction and competition terms that lead the contour towards object boundaries. CACE is much faster and more efficient in convergence than CPM. More importantly, it eliminates CPM's tendency to sometimes result in open contours. CACE also has significant advantages over the geodesic and GVF geodesic snakes in that it is more robust to initial placement and is able to handle objects of more complicated topology, e.g. those with narrow parts.

As electrostatics is the starting point of our work, we will review its key concepts in Section 2, along with a brief introduction to CPM and its shortcomings. In Section 3, the construction of our proposed model is discussed, with experimental results shown in Section 4. Section 5 concludes our work.

2 Background

An electrostatic field $\mathbf{E}$ is defined as the electrostatic force upon a unit charge due to other charges. Suppose there is a distribution of N point charges $c_1, c_2, \cdots, c_N$ fixed at locations $\mathbf{r}_1, \mathbf{r}_2, \cdots, \mathbf{r}_N$ respectively in a 2D space. According to Coulomb's Law, the electrostatic field at location $\mathbf{x}$ in this 2D domain is given as:

$$\mathbf{E}(\mathbf{x}) = \sum_{i=1}^{N} \frac{c_i}{4\pi\epsilon_0} \frac{\mathbf{x} - \mathbf{r}_i}{|\mathbf{x} - \mathbf{r}_i|^3}, \quad \mathbf{x} \in \mathbf{X}, \tag{1}$$

where ϵ_0 is the permittivity of free space and $\mathbf{X}$ is the set of all possible locations in this 2D domain. Thus $\mathbf{E}$ is a vector field that has a force at every location in $\mathbf{X}$. If a test charge e is placed in the field at location $\mathbf{x}$, the electrostatic force put upon it can be obtained by:

$$\mathbf{F}(\mathbf{x}) = e\mathbf{E}(\mathbf{x}). \tag{2}$$

It is important to note that the electrostatic force acting on the test charge e is merely the superposition of separate electrostatic forces imposed by every
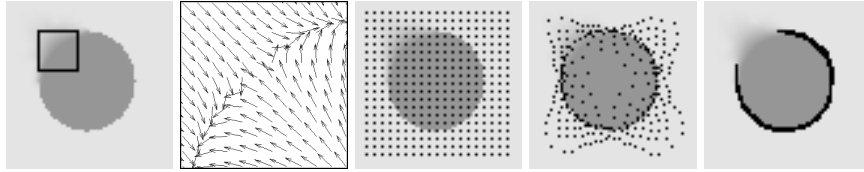
Fig. 1. Columnwise from left: synthetic circle image with highlighted weak edge area, the normalized Coulomb[1] force field in box area, initialized CPM, instance of particle movements, and the final CPM result.

fixed charge c_i. This implies that the force of charge c_i upon test charge e is not influenced by the presence of any other fixed charges in space. This principle enables us to compute forces from different sources separately and control their contribution to our charged contour model.

CPM [8] is a particle model built on the simulation of particle movements in an electrostatic field. A set of positively charged free particles is placed in a field distributed with negative fixed charges proportional to the input image edge strength. As the particles have the same polarity to each other, and opposite polarity to the fixed charges, an attracting image-based force is imposed on each particle by the fixed charges, while a repelling particle-based force is imposed by the particles upon each other[1]. These force are computed respectively using (2). Their normalised weighted sum, reduced by a damping factor, plays the role of acceleration for each particle. As the image-based force has larger weight than the particle-based force, the particles primarily move towards the nearest and strongest edges. The repelling forces then try to advance the particles along the boundary until they have reached an equilibrium state, thus detecting the entire boundary. A multiscale approach was used to partially alleviate the heavy computational costs, and also to allow particles quickly spread across the image domain at coarser levels to capture as many boundaries as possible.

The CPM model [8] benefits from initialisation that is largely insensitive to placement. Nevertheless, it is computationally intensive as (a) particles have to advance along boundaries in order to encompass the desired object, and (b) particles are added and deleted dynamically at each iteration. Although a damping factor is used to reverse the direction of acceleration when a particle crosses an edge, the particle will still move as long as its speed is not exactly zero, and therefore oscillations occur at the boundaries and particle convergence needs to be flagged by some criterion. Above all, CPM can not guarantee closed contours, inevitably resulting in gaps in the recovered object boundaries particularly if the object is occluded or has weak edges. Furthermore, a final reconstruction of points into curves for continuous representation of object boundaries is necessary which may not encapsulate the true boundary of the object. Fig. 1 shows a synthetic image of a circle with a blurred edge region indicated by a black

---

[1] In [8], the attractive force is referred to as the Lorentz force in the absence of a magnetic field, and the repellent force as the Coulomb force.

window. In such regions the image-based forces are significantly influenced by the stronger edges nearby (see vector field in Fig. 1). As the image-based forces always dominate the direction of movement, particles which have arrived at the weak edges will continue moving to the stronger edges with the weak edges left unmarked. This leads CPM to fail to close the border around the synthetic circle.

3 Proposed Model: Charged Active Contour Model based on Electrostatics (CACE)

The aim of our work is to improve on the drawbacks of the CPM particle model and the more traditional geometric contour models by integrating electrostatics principles with active contour evolution. Our proposed charged active contour model, CACE, detects objects starting with a *positively charged active contour* that propagates in an electrostatic field distributed with *negative fixed charges* proportional to image edge magnitudes.

The contour propagation in CACE results from the confluence of two components: a boundary attraction force and a boundary competition force. The attraction force acts as a bi-directional vector field which leads each point on the contour towards the boundaries from both sides. The competition force exerts most influence once any part of the snake reaches a boundary. It repels *free* contours nearby from reaching the already occupied boundary. The stronger the boundary, the larger the repelling force the contour exerts. This repelling force is also designed in a way such that only contours in homogeneous regions are most affected. In other words, contours that reach object boundaries will exert repellent forces upon other contours while they themselves will be least affected by others. At the same time, contours in homogeneous regions will continue to deform according to both attraction and competition forces. This is significantly different from the repelling force in the CPM model where the particles are constantly pushing each other in opposite directions. The electrostatic force field in the proposed CACE model is dynamically adapting as the contour evolves. This brings flexibility in initialisation and better curve propagation towards object boundaries. The CACE model is implemented in a geometric contour propagation framework using the Level Set representation to naturally handle topological changes.

We now describe in detail how these two forces are obtained and how they interact to create the joint electrostatic force field for the propagation of CACE.

3.1 Boundary attraction force field

Let I denote an image and $\mathbf{x}$ the pixel position. We use the Gaussian-based edge detector, with zero mean and variance σ_E, used in [7] as the boundary descriptor:

$$f(\mathbf{x}) = 1 - \frac{1}{\sqrt{2\pi}\sigma_E} \exp(-\frac{|\nabla(G_\sigma * I)(\mathbf{x})|^2}{2\sigma_E}), \quad \mathbf{x} \in \mathbf{X}. \tag{3}$$

where $G_\sigma * I$ denotes the convolution of the input image and a Gaussian smoothing kernel. The construction of the attraction force is based on the electrostatic force interaction as given in (1) and (2). Here, we treat the boundary pixels, defined in (3), as fixed negative charges with magnitude proportional to their edge strength. Thus, given N as the number of negative charges at locations $\mathbf{r}_1, \mathbf{r}_2, \cdots, \mathbf{r}_N$ across the edge map then the negative charge assigned to each edge pixel $\mathbf{r}_i$, denoted as $q_{\mathbf{r}_i}$ and simplified to q_i, is $q_i = -f(\mathbf{r}_i) < 0$.

The electrostatic field $\mathbf{E}_A(\mathbf{x})$ generated by these negative fixed charges can then be computed according to (1) as:

$$\mathbf{E}_A(\mathbf{x}) = \sum_{i=1}^{N} \frac{q_i}{4\pi\epsilon_0} \frac{\mathbf{x} - \mathbf{r}_i}{|\mathbf{x} - \mathbf{r}_i|^3}, \quad \mathbf{x} \in \mathbf{X}. \tag{4}$$

This electrostatic vector field points towards the negative fixed charges, i.e. the edges, resulting in a bi-directional force field. The snakes can be hypothesised as positive charges moving in the image domain under the influence of the negative boundary charges with the aim of converging towards them from both sides. Let M be the number of positive charges at positions $\mathbf{s}_1, \mathbf{s}_2, \cdots, \mathbf{s}_M$ on the contour, and $p_{\mathbf{s}_j}$, simplified to p_j, denote the positive charge assigned to point $\mathbf{s}_j$. The attractive electrostatic force $\mathbf{F}_A$ enforced upon the contour is then:

$$\mathbf{F}_A(\mathbf{s}_j) = p_j \mathbf{E}_A(\mathbf{s}_j), \quad \mathbf{s}_j \in \mathbf{X}. \tag{5}$$

As the contour and the fixed charges have opposite polarity, the electrostatic boundary attraction force continuously pushes the contour towards object boundaries. In this study, a constant unit positive charge p_j is assigned to all snake points. However, p_j can be treated as a variable for other applications.

3.2 Boundary competition force field

While the boundary attraction force is constantly pushing the snake towards boundaries, the boundary competition force allows progress only towards unoccupied object boundaries. It helps a snake already occupying an object boundary to check the advance of free contours nearby.

The competition force results from an electrostatic field which continuously adapts as the contour evolves and reaches boundaries. Two conditions characterise this force: (a) Contours that are on the object boundaries endow most to the electrostatic field with contributions proportional to the edge strength. (b) The force upon a contour due to this electrostatic field is proportional to the inverted strength of the edge covered by this contour. In other words, contours in homogeneous regions are most enforced upon while those on top of strong edges are least pushed. This ensures the snakes stay at their detected boundaries but push away nearby snakes competing for the same boundaries.

Condition (a) above is realised by weighting the contour charges with the edge function, i.e. $p_j' = f(\mathbf{s}_j)p_j$. The resulting electrostatic field comprises vectors

pointing away from the edges already occupied by contours. It is given as:

$$\mathbf{E}_C(\mathbf{x}) = \sum_{j=1}^{M} \frac{p_j'}{4\pi\epsilon_0} \frac{\mathbf{x} - \mathbf{s}_j}{|\mathbf{x} - \mathbf{s}_j|^3} = \sum_{j=1}^{M} \frac{f(\mathbf{s}_j)p_j}{4\pi\epsilon_0} \frac{\mathbf{x} - \mathbf{s}_j}{|\mathbf{x} - \mathbf{s}_j|^3}, \quad \mathbf{x} \in \mathbf{X}. \tag{6}$$

Condition (b) is realised by weighting the contour charges with an edge stopping function, i.e. $g(.) = 1 - f(.)$, to generate the boundary competition force $\mathbf{F}_C$:

$$\mathbf{F}_C(\mathbf{s}_j) = g(\mathbf{s}_j)p_j\mathbf{E}_C(\mathbf{s}_j), \quad \mathbf{s}_j \in \mathbf{X}. \tag{7}$$

Thus, $\mathbf{F}_C$ can be considered as a boundary competition force that prevents contours from approaching the same boundaries. For example, consider point charges p_a and p_b on the active contour at positions $\mathbf{s}_a$ and $\mathbf{s}_b$. If these two points are both in homogenous regions, $\mathbf{E}_C(\mathbf{s}_a)$ and $\mathbf{E}_C(\mathbf{s}_b)$ are small, and they exert little competition force upon each other (and on other snake points). However, both of them are repelled by any other points that have already reached boundaries. When one of this pair, say p_a, reaches a boundary, it (along with all other snake points on object boundaries) will alter the electrostatic field according to (6), with its contribution to the field being proportional to its edge strength $f(\mathbf{s}_a)$. The impact of this electrostatic field on p_a itself is however minimised since the force $\mathbf{F}_C(\mathbf{s}_a)$ is weighted by $g(\mathbf{s}_a)$ (in (7)), i.e. the stopping function prevents it from being pushed away from the boundary. The snake point p_b on the other hand provides little contribution to this field, but will be most affected by the competition force $\mathbf{F}_C(\mathbf{s}_b)$ due to the large value of $g(\mathbf{s}_b)$ in the homogeneous region. When both snake points reach a boundary, they both contribute to the electrostatic field but have barely any influence on each other.

3.3 Joint electrostatic force

The joint electrostatic force $\mathbf{J}$ on the active contour is obtained by combining (5) and (7) as such:

$$\begin{aligned}
\mathbf{J}(\mathbf{s}_j) &= p_j[\lambda\mathbf{E}_A(\mathbf{s}_j) + (1 - \lambda)g(\mathbf{s}_j)\mathbf{E}_C(\mathbf{s}_j)] \\
&= \lambda\mathbf{F}_A(\mathbf{s}_j) + (1 - \lambda)\mathbf{F}_C(\mathbf{s}_j).
\end{aligned} \tag{8}$$

The real positive constant λ balances the contribution between the boundary attraction force and the boundary competition force. As shown in sections 3.1 and 3.2, the first term attracts the contours to object boundaries, while the second term prevents the contours from approaching the boundaries that are already covered by other contours. The ever-changing force field causes the free contours to change direction and search for other boundaries.

It is important to further emphasise that the joint force field is dynamically adapting to the evolution of the snake and in turn defining its advance. The electrostatic attraction force field described in Section 3.1 is a *static* bi-directional vector field that attracts contours to object boundaries. A deformable contour model solely based on this static force field inevitably suffers from similar difficulties as the GVF snake model and its variations. Instead of attempting to
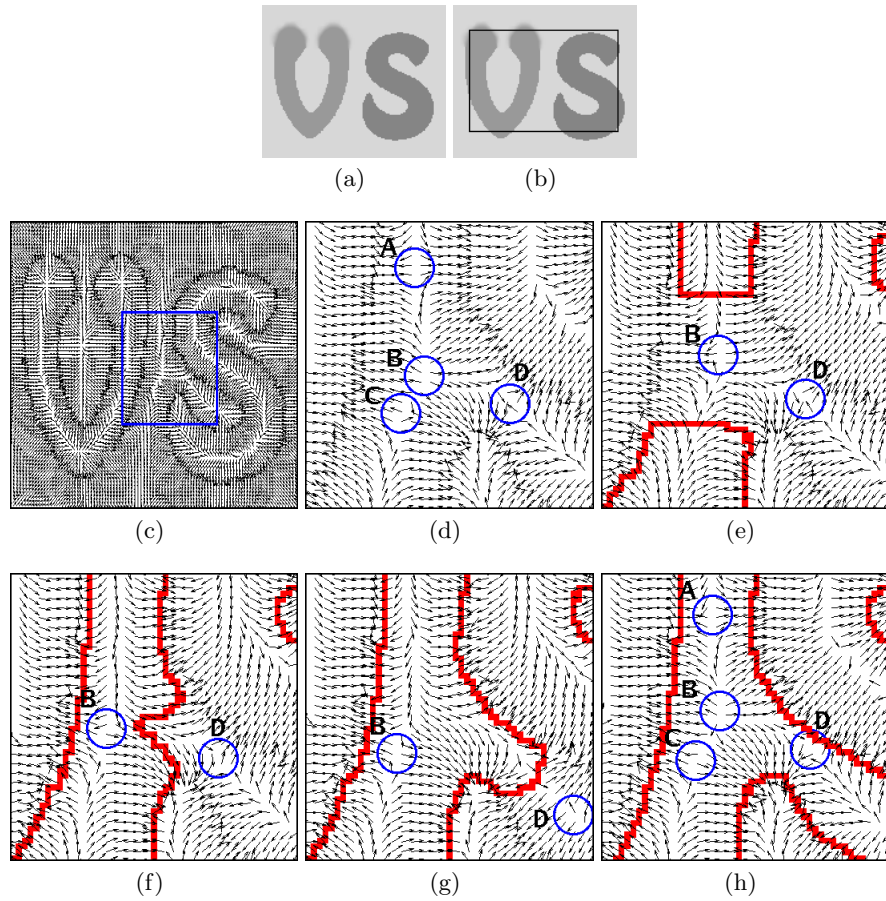
Fig. 2. Change of force fields during contour propagation. (a) Test image with letters 'V' and 'S'; (b) Initial snake; (c) Initial CACE vector field with marked region; (d) Closeup view of the vectors in the marked region in the valley between 'V' and 'S'; (e)-(f) Adapting vector field as snake progresses. Snake positions are indicated in thick dark red, and critical points are shown in thin blue circles.

overcome the saddle or divergent points in a vector field as proposed in [7], the CACE model adapts the vector field through the boundary competition force so that such critical points change as the snake approaches.

Fig. 2 illustrates adaptive changes of the joint electrostatic force field during contour propagation. The test image and the initial CACE snake are shown in 2(a) and 2(b) respectively. Fig. 2(c) shows the initial vector force field and Fig. 2(d) is a closeup of the square region marked in 2(c) in the valley between the letters 'V' and 'S'. There are four critical points, indicated by thin blue circles, that can stop the snake from further propagation. A, C, and D are saddle points, while B is a divergent point. The thick red contours in Figs. 2(e)-2(h) are the

progressing positions of the CACE snake. In 2(e), as the snake evolves in the valley, the saddle points A and C disappear. Notably, the divergent point B becomes a saddle point. Saddle point D stays approximately the same, as the snake is still far away from it. In 2(f), the snake has just passed the valley and is going to enter the deep concave in the letter 'S'. In 2(g) the saddle point D is clearly moving away from the entrance of the concavity as the snake approaches. Finally in 2(h), the snake reaches the boundaries and the vector field takes a similar form as the initial state. The saddle points A and C re-emerge, saddle point D is back to the entrance of the concave, and B changes back into a divergent point. The corresponding CACE evolutions are shown in the last row of Fig. 4.

3.4 Geometric active contour formulation for CACE

Let C be the active contour. The contour evolution formulation for the CACE model is defined as:

$$C_t = \alpha g \kappa \mathcal{N} + (1 - \alpha)(\mathbf{J} \cdot \mathcal{N})\mathcal{N}, \tag{9}$$

where α is a real constant, κ denotes the curvature, and $\mathcal{N}$ is the unit inward normal. The first term regulates the contour, and the second term attracts the snake towards the object boundaries. To ensure efficient contour propagation, we normalize the force field along the contour normal by replacing the term $(\mathbf{J} \cdot \mathcal{N})\mathcal{N}$ with $\frac{(\mathbf{J} \cdot \mathcal{N})\mathcal{N}}{|(\mathbf{J} \cdot \mathcal{N})\mathcal{N}|}$.

To achieve topological flexibility, we use level sets [9] to represent the contour, implicitly evolving it by deforming the level set function, u. This involves two extensions. The first is to embed the 2D contour into a 3D level set function u, which is achieved by using the signed distance transform such that the embedded snake is given by the zero level set at any time. The second is to extend the force field defined on the 2D contour to the 3D level sets. The Fast Marching Method can be used to accomplish this as proposed in [10]. However, in this study, we can simply compute the extended force field by treating each level set as a deforming contour at each time step. Thus, the joint force field $\mathbf{J}(\mathbf{s}_i)$ as given in (9) is extended to $\mathbf{J}(\mathbf{x})$ across the image domain. Thus, given the fact that $\mathcal{N} = -\frac{\nabla u}{|\nabla u|}$, the level set representation of our CACE snake is given as:

$$u_t = \alpha g \kappa |\nabla u| - (1 - \alpha)\mathbf{J} \cdot \nabla u. \tag{10}$$

4 Experimental Results

In this section we present results for our CACE model and compare its performance against the CPM, the geodesic contour, and the GVF geodesic contour models. The software for all the methods we compare against was developed in-house based on the relevant literature, i.e. [8, 7, 11].

CACE copes much better than CPM when faced with weak edges (cf. Fig. 3 with Fig. 1). As CPM particles arrive at weak edges, they carry on moving

towards stronger edges along the boundaries, hence fail to correctly recover the object boundaries. CACE stabilizes around the boundaries, successfully detecting the whole object, due to the bi-directional nature of its force field and the characteristics of the contour itself. The vectors pointing towards the edges, although weak, prevent leakage from both sides.
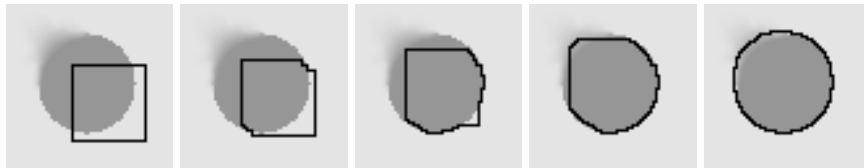

Fig. 3. Propagation of CACE on disc object with weak edges (cf. with Fig. 1).

CACE possesses significant advantages over other contour models, e.g. it is more robust to initial placement than the geodesic snake, and better capable of handling object topology than the GVF geodesic snake, as shown in Fig. 4. While the geodesic snake fails to detect the objects under initialization that crosses boundaries, the GVF geodesic snake is less constrained, but nonetheless, still unable to reach some of the boundaries when it gets trapped by divergent vectors in homogeneous areas. CACE improves on these limitations and succeeds in detecting both objects in Fig. 4.

Fig. 5 shows the evolution process in CPM, geodesic snake, GVF geodesic snake, and CACE, on a corpus callosum detection task in an MRI brain image. Although the coarse-to-fine multi-scale setting is used, CPM still fails to recover the corpus callosum, as particles can not advance from stronger boundaries towards weaker ones and are thus blocked in the area where strong edges occur. The geodesic snake also fails in the detection task due to initialization across boundaries, as does the GVF geodesic snake which gets trapped by saddle points formed within the corpus callosum. In comparison, CACE benefits from the self-adaptive nature of the force field and manages to propagate through the elongated part of the object and capture the entire boundary.

Figs. 6 and 7 show more examples where CACE again performs more accurately than the other snake models under highly noisy and textured conditions.

The CACE model performs well on a range of parameter settings. Two main parameters are involved: (λ, α). The parameter λ in (9) balances the contribution between the attraction and the competition forces. We set $\lambda = 0.3$ throughout our experiments determined empirically for the set of images shown. The parameter α controls the smoothness of the contour and has minor impact on the model performance and was kept constant at $\alpha = 0.1$ throughout our work.

It is worth noting that the computation of the electrostatic force field in (4) or (6) is simple but inefficient, requiring $O(N^2)$ computational complexity and increases drastically as the image size increases. Therefore, as with CPM in [8], we use the Particle-Particle Particle-Mesh method, originally proposed in [12],

for fast and accurate evaluation of the electrostatic field. Details of the method can be found in [12]. In terms of comparative computational performance, we used a 200×200 image in which all models successfully found the object. Using a 2.8 GHz Linux PC running uncompiled Matlab code, the computational times for the different particle and contour models were as follows: 281s for CPM, 26s for the geodesic snake, 20s for the GVF geodesic snake, and 29s for CACE.

5   Conclusion

In this paper, we presented a novel active contour model, namely the Charged Active Contour, CACE. It incorporates electrostatics principles from the CPM particle model [8] into the deformable contour model. The CACE snake deforms under the confluence of an external boundary attraction force and an external boundary competition force. Driven by this combined electrostatic force, contours move towards object boundaries, and will end up there if the boundaries are not covered by other contours, or change direction and search for other boundaries otherwise.

Experimental results have demonstrated that by introducing particle dynamics into the contour model, the snake can be more initialisation independent, exhibit better ability in reaching concavities, and ensure closed contours.
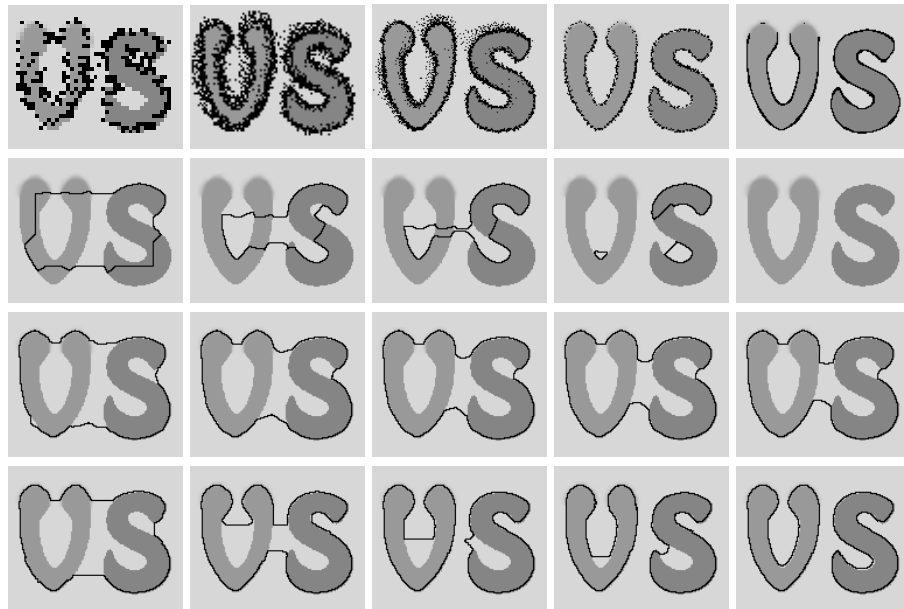

Fig. 4. Contour propagation for boundary detection. Top row: iterations of the CPM, 2nd row: geodesic snake, 3rd row: GVF geodesic snake, final row: CACE
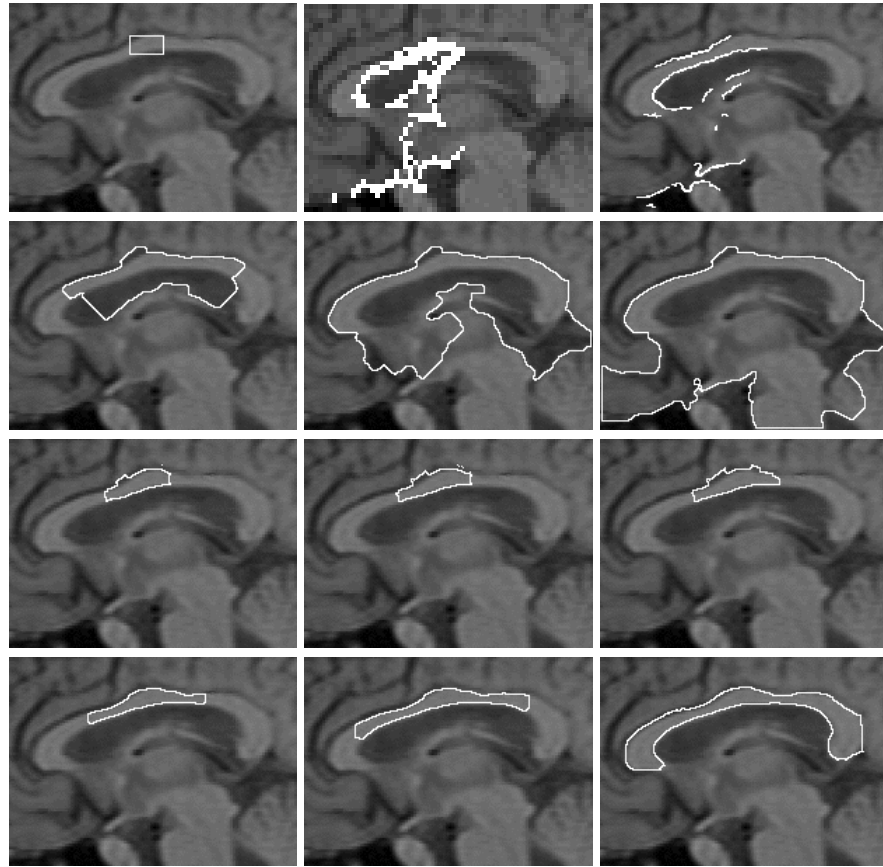
Fig. 5. From left to right, top: input image and initialisation for all the models, iteration of the CPM, final CPM result, 2nd row: evolution of the geodesic snake, 3rd row: evolution of the GVF geodesic snake, final row: evolution of CACE

.

References

1. Kass, P., Witkin, A., Terzopoulos, D.: Snakes: Active contour models. IJCV **1** (1988) 321–331
2. Caselles, V., Kimmel, R., Sapiro, G.: Geodesic active contours. In: ICCV. (1995) 694–699
3. Zhu, S., Yuille, A.: Region competition: Unifying snakes, region growing, and Bayes/MDL for multiband image segmentation. IEEE T-PAMI **18** (1996) 884–900
4. Paragios, N., Deriche, R.: Geodesic active regions for supervised texture segmentation. In: ICCV. (1999) 926–932
5. Xie, X., Mirmehdi, M.: RAGS: Region-aided geometric snake. IEEE T-IP **13** (2004) 640–652
6. Xu, C., Prince, J.: Gradient vector flow: a new external force for snakes. In: CVPR. (1997) 66–71
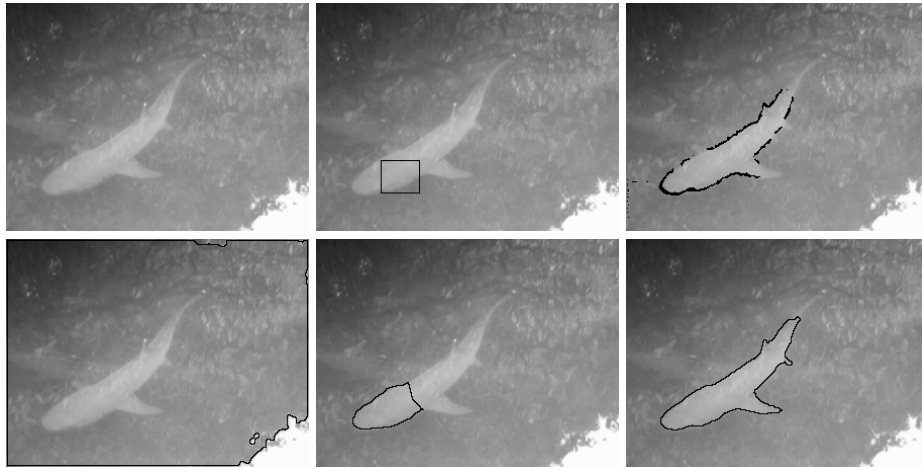
Fig. 6. From left to right, top: noisy input image, initialization for all models, CPM results, and bottom: results for the geodesic snake, the GVF geodesic snake, and CACE.

Fig. 7. From left to right, top: input image, initialization for all models, CPM results, and bottom: results for the geodesic snake, the GVF geodesic snake, and CACE.

7. Paragios, N., Mellina-Gottardo, O., Ramesh, V.: Gradient vector flow fast geodesic active contours. IEEE T-PAMI **26** (2004) 402–407
8. Jalba, A., Wilkinson, M., Roerdink, J.: CPM: A deformable model for shape recovery and segmentation based on charged particles. IEEE T-PAMI **26** (2004) 1320–1335
9. Sethian, J.: Level Set Methods: Evolving Interfaces in Geometry, Fluid Mechanics, Computer Vision, and Materials Science. CUP (1996)
10. Adalsteinsson, D., Sethian, J.: The fast construction of extension velocities in level set methods. J. Comp. Phy. **148** (1998) 2–22
11. Caselles, V., Catte, F., Coll, T., Dibos, F.: A geometric model for active contours. Numerische Mathematik **66** (1993) 1–31
12. Hockney, R., Eastwood, J.: Computer Simulation Using Particles. Taylor and Francis (1988)